# Size effect in two-dimensional oxide-on-metal catalysts of CO oxidation and its connection to oxygen bonding: An experimental and theoretical approach

Ke Zhang, Linfei Li, Jacek Goniakowski, Claudine Noguera, Hans-Joachim Freund, Shamil Shaikhutdinov

# Size effect in two-dimensional oxide-on-metal catalysts of CO oxidation and its connection to oxygen bonding: An experimental and theoretical approach

Ke Zhang,[#] Linfei Li, [#] Jacek Goniakowski,* Claudine Noguera

Hans-Joachim Freund, Shamil Shaikhutdinov*

**Abstract**

Transition metal oxide layers on metal surfaces often show superior catalytic performance as compared to conventional, i.e., metal-on-oxide, systems. In this work, we studied the CO oxidation reaction over FeO supported by Pt(111) and observed strong size effects on the reactivity. The monolayer islands below 5 nm in size showed a light-off temperature for $CO_2$ production 200 K lower than for the 30 nm islands. In an attempt to rationalize the size effect, we have performed oxygen desorption experiments and have combined them with an extended DFT analysis to provide insight into the bonding of various oxygen species in such systems. The theoretical results on isolated $FeO_2$ islands indicate a substantially lower stability of the boundary oxygen atoms as compared with the same islands embedded into an FeO layer in qualitative agreement with experiment showing that the smaller the island, the lower the desorption temperature. To the best of our knowledge, the results demonstrate the first example of a size effect in oxidation catalysis on *two-dimensional* systems**.**

**Keywords:** CO oxidation; monolayer catalysts; iron oxide; metal/oxide interface.

[#] These authors contributed equally to the work.

## 1. Introduction

Transition metal oxides (TMO) are active players in catalysis, in particular in oxidation reactions. The differentiation of the various oxygen species in activity is important and, therefore, needs speciation. This concept has been propagated prominently by Robert Grasselli [1, 2] with respect to oxidation of hydrocarbons on complex oxides, as well as by Jerzy Haber combining theory and experiment.[3-5] Even in the case of supported metal catalysts, where the noble metal particles are supported on a TM-oxide, the role of the oxide support often extends beyond that of being solely a template to fix the metal component, in that it actively participates in the process. A notable special case is represented by the so-called "Strong Metal Support Interaction" (SMSI), where the metal oxide may overgrow the supported metal particle and thus affect catalytic performance.[6] A detailed understanding of SMSI, whether it involves structural and/or electronic effects, remains under debate.[4, 7-10] SMSI often manifests itself *via* encapsulation of metal nanoparticles by a very thin oxide film stemming from a TMO support. Therefore, establishing the structure-reactivity relationships for *ultrathin* TMO films on metals may shed light on the SMSI effects.[11] In particular, the nature of oxygen species in the TMO films and its role in the oxidation reactions need to be better understood.

The interest in such studies increased after a "monolayer" FeO(111) film on Pt(111) was found to be active in low temperature CO oxidation, [12] and this is the film that encapsulates Pt nanoparticles supported on $Fe_3O_4$ as result of SMSI.[13, 14] However, under reaction conditions at near atmospheric pressures, the FeO(111) film transforms into the "O-rich" film with a compositional stoichiometry close to $FeO_2$ (henceforth referred to as a $FeO_{2-x}$ film). Due to the Moiré-like coincidence structure formed on the initial FeO(111)/Pt(111) surface,[15] the O-rich film has a complex structure. Based on scanning tunneling microscopy (STM) studies [12] and density functional theory (DFT) calculations [16, 17], the film forms close-packed O-Fe-O trilayer islands, following the Moiré pattern, with an ill-defined structure between the islands. Temperature

programmed desorption (TPD) measurements showed that the $FeO_{2-x}$ films contain oxygen species desorbing at much lower temperatures than in FeO. Weakly bound oxygen (WBO) species were attributed to the O atoms in the topmost layer. Accordingly, it is this oxygen that reacts with CO to form $CO_2$. Comparison with other TMO films tested in this reaction suggested that the binding energy of WBO species, determined by TPD, may serve as a descriptor for this reaction.[18]

At sub-monolayer oxide coverages, the oxide/metal interface starts to dominate the reactivity. Indeed, the $CO_2$ production rate increases and apparently follows the total island perimeter length, both reaching a maximum at mid-coverages.[19, 20] It was reasonably thought that CO strongly adsorbing on Pt reacts with the O atoms at the oxide island edge, either on the FeO/Pt [21] or $FeO_2$/Pt,[19] depending on reaction conditions. However, a more recent study [22] provided evidence for the steady state reaction taking place neither on FeO/Pt nor $FeO_2$/Pt interfaces, but at the boundary between oxidized and reduced phases of the iron oxide film formed under reaction conditions. In this scenario, the metal (Pt) surface solely aids in the initial formation of such boundaries close to the island edges rather than directly participates in the reaction.

In this work, we report substantial size effects of FeO islands on the CO oxidation reaction. Reducing the island size down to 5 nm considerably lowers the light-off temperature for $CO_2$ production. In an attempt to rationalize this effect, we have performed oxygen desorption experiments and have combined them with an extended DFT analysis to provide insight into the bonding of various oxygen species on such systems. The theoretical results on isolated $FeO_2$ islands indicate a substantially lower stability of the boundary oxygen atoms as compared with the same islands embedded into an FeO layer in qualitative agreement with experiment showing that the smaller the island, the lower the desorption temperature. To the best of our knowledge, the results demonstrate the first example of a size effect in oxidation catalysis on *two-dimensional* systems**.**

## 2. Methods and Materials

*2.1 Experimental Section*

The experiments were carried out in several UHV chambers (base pressures below $5\times10^{-10}$ mbar) all equipped with standard facilities for cleaning the Pt(111) single crystal surface and preparation of the FeO(111) films. *In situ* STM studies were performed using a variable-temperature scanning tunneling microscope (VT-STM, Omicron). Temperature programmed reaction (TPR) measurements were performed in another chamber using a quadrupole mass-spectrometer (QMS, from Pfeiffer). The prepared samples were characterized with Omicron VT-STM/AFM at room temperature. Oxygen desorption experiments were performed in the third UHV chamber equipped with STM (Omicron) and QMS (Hiden).

In all setups, Fe was deposited using e-beam assisted evaporator (Focus EMT3) from an Fe rod (99.9999%, Sigma Aldrich). FeO(111) islands were prepared by Fe deposition onto a clean Pt(111) substrate in $10^{-7}$ mbar of $O_2$ at room temperature, followed by annealing in $10^{-6}$ mbar $O_2$ at 700 K for 5 min. In order to prepare the smallest FeO(111) islands, Fe was deposited onto a substrate kept at 100 K. The samples were then oxidized in $10^{-5}$ mbar $O_2$ at 573 K to transform FeO(111) into the $FeO_{2-x}$ phase.

*Computational Methods*

All DFT calculations were performed with the Vienna Ab-initio Simulation Package (VASP),[23, 24] using Projector Augmented Wave (PAW) method [25, 26] to represent the electron-core interaction, and the Perdew-Wang 91 (PW91) [27] gradient-corrected exchange-correlation functional. Following our previous studies,[28, 29] iron oxides were treated with the DFT+U approach in the form proposed by Dudarev,[30] with $U_{Fe} - J_{Fe} = 3$ eV. $FeO_X$/Pt(111) system was represented by a three-layer-thick Pt(111) slab with the $FeO_X$ oxide adsorbed on one side only. The bottom Pt layer was hold fixed while the two surface Pt layers and the oxide film were fully relaxed (threshold on forces equal to 0.01 eV/Å). The slabs were separated by at least 10 Å of vacuum and the dipole corrections were

applied in order to eliminate the residual dipoles in the direction perpendicular to the surface. In order to take into account the effect of lattice mismatch between the Pt(111) substrate and the oxide layer and to mimic the coincidence structures observed experimentally,[31] a ($\sqrt{73} \times \sqrt{73}$)R5.8°-FeO(111)//($\sqrt{91} \times \sqrt{91}$)R5.2°-Pt(111) periodic supercell has been used. Its large size makes Γ point sufficient to sample the Brillouin zone. Following our previous studies, soft oxygen pseudopotential (energy cutoff of 280 eV) was used and a row-wise anti-ferromagnetic alignment of Fe spins was systematically imposed. [19, 32] Atomic charges were estimated with the partition scheme proposed by Bader, [33, 34] and atomic configurations were plotted with VESTA.[35]

## 3. Results and Discussion

*Experimental results*

We first show how CO interacts with the $FeO_{2-x}$ islands using *in situ* STM. Figure 1 displays STM images continuously recorded in $10^{-6}$ mbar of CO at 350 K for different exposure time as indicated. Regular protrusions imaged on the island surface reflect O-Fe-O trilayer domains showing the same periodicity (2.5 nm) as the Moiré structure in the original FeO(111)/Pt(111) films. Obviously, the reaction starts at the edge and propagates towards the center of the island until all $FeO_2$ related protrusions disappear due to their reduction back to FeO layer. Although STM tip effects cannot be ruled out, the reduced surface does not look atomically flat because the temperature (350 K) may not be high enough for complete structural relaxations accompanying the oxide reduction. Interestingly, the time required for CO to reduce $FeO_2$ domains at the perimeter is considerably shorter than that obtained for reduction of the next “spots ring” left (about 20 and 70 min, respectively). This finding suggests that the $FeO_2$ domains close to the island edge are much more reactive to CO than those located in the interior region of the island upon reaction front propagation. Henceforth, we referred to those as the “edge” and the “interior” spots, respectively.

Not surprisingly, the observed reaction is a thermally activated process. It proceeds much faster at increasing temperature. In order to get an estimate for the activation barrier, we imaged identically prepared samples all exposed to $10^{-6}$ mbar CO at several different temperatures between 300 and 450 K. In a crude approximation, we assume that the reaction rate is inversely proportional to the time ($\tau$) needed for depleting the "edge" $FeO_2$ spots. The rate *vs* temperature dependence showed Arrhenius-like behavior (Figure 1), from which we calculated the apparent activation energy of ~40 kJ/mol. The energy barrier can be assigned to the CO + O -> $CO_2$ reaction step, which is considered as the rate-limiting step in the CO oxidation reactions following Mars-van Krevelen type mechanism.

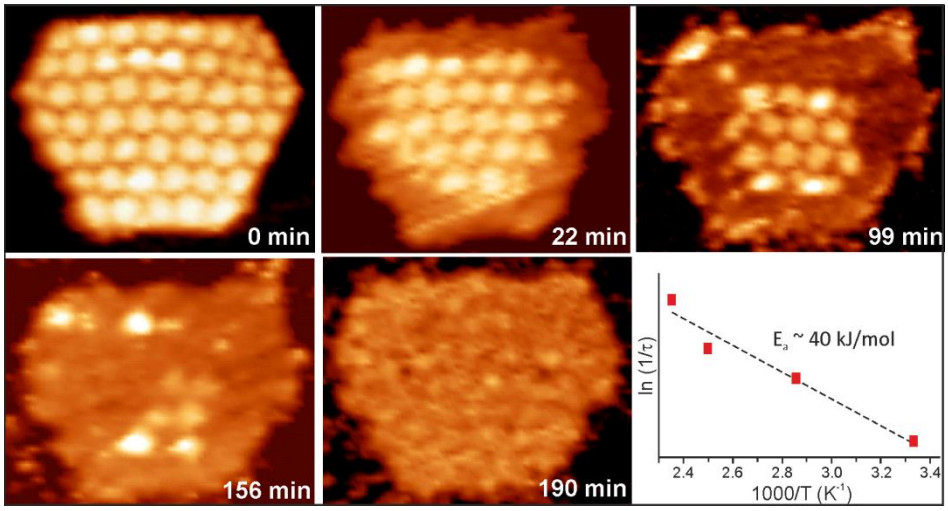


**Figure 1.** *In situ* STM images of an individual $FeO_{2-x}$ island recorded in $10^{-6}$ mbar of CO at 350 K. Exposure time is indicated. (The image size is 24 nm × 20 nm; tunneling parameters: -2 V, 0.1 nA.) The panel shows the Arrhenius plot for the initial rate of reduction (measured by STM *ex situ*) as a function of temperature (300 - 450 K).

This high reactivity of $FeO_2$ spots at the island edge further manifested itself in the temperature programmed reduction (TPR) experiments summarized in Figure 2. Upon heating a sample in $10^{-6}$ mbar of CO, the latter reduces $FeO_{2-x}$ to FeO producing $CO_2$ that has been recorded by a mass-spectrometer. The sample (1) has been prepared in such a way that it primarily exposes islands containing only "edge" spots as shown in the corresponding STM image. The maximum in $CO_2$ production on this sample is observed at

375 K. Then the sample was annealed in UHV at 650 K for 30 min to promote oxide sintering and re-oxidized in $O_2$ to transform islands back into the O-rich, $FeO_{2-x}$ phase (sample 2) before the new TPR run. The procedure was repeated to prepare the samples (3) and (4). The morphology of each sample was inspected by STM before and after the TPR experiment.

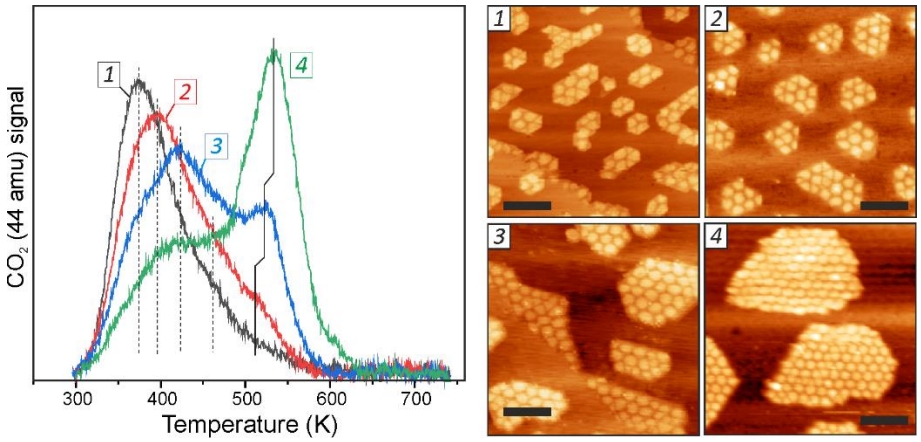


**Figure 2.** Temperature programmed reduction profiles measured on $FeO_{2-x}$/Pt(111) samples (1-4) shown in STM images (the scale bars are 10 nm) taken prior to the TPR run. The spectra are obtained by recording the $CO_2$ (44 amu) mass-spec signal in $10^{-6}$ mbar of CO upon linear heating with the rate 2 K/s.

It should be mentioned that the O ad-atoms remaining on the Pt(111) surface after sample preparation (exposure to $5\times10^{-6}$ mbar $O_2$ at 573 K for 10 min, then pumping out and cooling to 300 K) readily react with residual CO in the UHV background during STM imaging and hence do not contribute to the $CO_2$ signal measured. Indeed, the four TPR spectra are very different, whereas the integral $CO_2$ signal area remains the same since the total oxide coverage is not changed upon islands sintering, but the island size.

TPR profiles revealed certain correlation with the sample morphology imaged by STM. It is clear that reaction at the lowest temperature occurs on the smallest islands exposing solely "edge" $FeO_2$ spots. As the island size increases, the total number of such spots decreases, and its contribution to overall $CO_2$ production diminishes. Concomitantly, the TPR profile shifts to higher temperatures, which is associated with the reaction propagating into the islands interior, as directly shown by *in situ* STM (Figure 1). Although

the low-temperature peak shifts to higher temperatures (from 375 to 420 K in samples (1)-(4), respectively), it seems to consist of several discrete components (indicated by dashed lines to guide the eye), each associated with the certain island size. Meanwhile a high-temperature signal is represented by one peak, albeit slightly shifting (from 510 to 535 K) at increasing size. Therefore, the combined TPR and STM results point out a strong size effect on CO reaction with O in oxide: The smaller the islands, the lower the light-off temperature and hence the activation energy for $CO_2$ formation.

In an attempt to rationalize exceptional activity of the "edge" $FeO_2$ spots and assuming that the binding energy of WBO species remains the descriptor for CO oxidation on partially covered films as well, we studied oxygen desorption using TPD. Figure 3a shows TPD spectra measured on $FeO_{2-x}$/Pt(111) films of three different coverages, *i.e.*, 0.25 , 0.5 and 1 ML (the latter corresponds to a dense monolayer (ML) film), determined from STM images shown as insets. Negligible oxygen desorption was detected on the FeO-free Pt(111) sample under the same preparation conditions, most likely due to the reaction with CO in the UHV background. The presented spectra show solely oxygen evolution during thermal reduction of the oxidized $FeO_{2-x}$ phase into FeO, which, in turn, decomposes at temperatures as high as 1200 K.[12] The spectra clearly show that: (i) the signal intensity is proportional to the oxide coverage; (ii) the entire desorption profile shifts to higher temperatures with increasing coverage and/or island size; (iii) the desorption signals are highly symmetric and almost identical in shape.

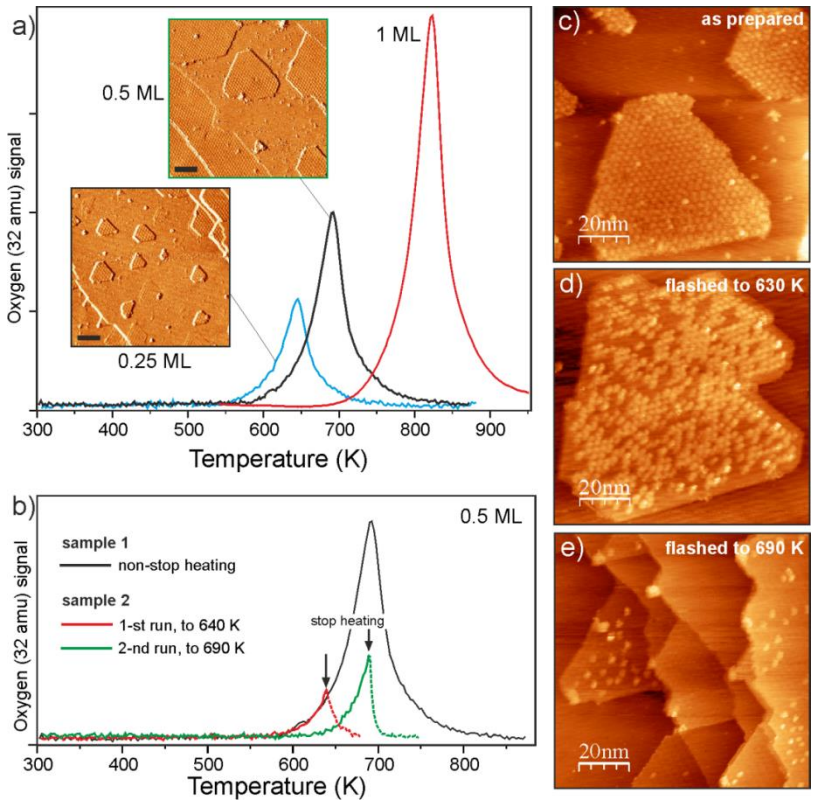


**Figure 3.** (a) $O_2$ (32 amu) TPD spectra recorded on $FeO_{2-x}$/Pt(111) at three different film coverages as indicated. STM images of the "as prepared" 0.25 and 0.5 ML samples (presented in the differentiated contrast) are shown in inset. The scale bar is 20 nm. (b) Black line reproduces the TPD spectrum for the 0.5 ML sample (1) from panel a). The newly prepared 0.5 ML sample (2) was first heated to 640 K (red line) and imaged with STM at 300 K. Then the sample was heated to 690 K (green line) and inspected by STM again. Dashed lines show (inertial) desorption traces after heating was stopped. The heating rate in all spectra is 2 K/s. (c-e) STM images of the sample "as prepared" (c) and after heating to 640 K (d) and 690 K (e), respectively.

It is interesting, that such spectra resemble those previously reported for noble metal surfaces oxidized at strongly oxidizing conditions and often referred to as "explosive" desorption.[36-38] In particular on Pt(111), the desorption peak was found to shift from 700 K to 750 on increasing nominal O coverage from 1.5 ML to 2.9 ML, respectively.[37] Other values are reported in Ref. [36]: the peak shifts from 680 K at 1.8 ML to 710 K at 2.4 ML. In principle, desorption temperatures observed in Figure 3a fall in the range obtained on oxidized Pt(111) surfaces. The $O_2$ desorption spectra on Pt(111) were originally explained by considering the influence of surface tension on the decomposition rates of $PtO_x$ oxide particles presumably covering the surface.[36] As

particles increase in size, the rate at a given temperature decreases because the surface tension on the particles also decreases. Accordingly, the maximum desorption rate shifts to higher temperatures at increasing coverage. “Explosive” desorption occurs because as the particles shrink during decomposition they become increasingly less stable and hence decompose rapidly during the TPD experiments.

Such TPD behavior was later explained by a kinetic model in which O atoms migrate from oxide domains (“condensed phase”) onto the surface regions containing chemisorbed oxygen atoms (“dilute phase”).[37, 38] Desorption directly from the dense phase was considered to be negligible, and it preferentially occurred from the dilute phase, with the oxide islands and particles acting as a reservoir for O. The migration of species from the dense phase to the dilute phase was assumed to be faster than the desorption from either phase. Under these conditions, the desorption rate is proportional to the fraction of the surface covered by the dilute phase. Since this fraction increases as the dense phase is consumed, desorption is self-accelerating and the rate increases rapidly once desorption is initiated. Basically, explosive desorption occurs because the area of the surface from which species desorb, and hence the total desorption rate, increases until the dense phase is completely decomposed.

The latter mechanism seems hardly plausible for the case of FeO/Pt. First, on noble metal surfaces considered above, surface oxide domains (or particles) are fully reduced to the metal which is incorporated back to the metal surface. In our case, $FeO_{2-x}$ islands only undergo reduction to FeO and do not vanish, thus the area of dilute phase remains constant. Second, the O atoms have to migrate across the $FeO_x$ island to reach the perimeter. This step is not included in the above model, and no experimental results exist thus far to get an estimate for diffusion coefficients. Third, the amount of oxygen released during the $FeO_{2-x}$ -> FeO transformation is, at most, 0.8 ML with respect to Pt(111).[12] Once all these O atoms spread onto the clean Pt(111) surface surrounding oxide islands covering 25% of the surface (the 0.25 ML sample, see Figure 3a), the amount of O ad-atoms would only be sufficient to form a (2×2)-O ad-layer which normally desorbs at about 750 K, *i.e.*, considerably higher than 640 K observed on this sample. In addition, the

kinetic model assumes (2×2)-O as the critical O concentration for the dilute phase, that must be *sustained via* dissolution of oxide phase.

To gain more insight into oxygen desorption from our films, we studied morphology of the 0.5 ML sample by STM after heating was stopped at 640 K, *i.e.*, shortly after the $O_2$ desorption starts. In the next run, the sample was heated to 690 K, that is the maximum desorption temperature, and again inspected by STM. Desorption traces are shown in Figure 3b together with the one obtained by non-stop heating to 900 K (replotted from Figure 3a) for direct comparison.

At first glance, comparison of STM images before and after heating to 640 K (Figure 3c,d) shows rather random disappearance of the $FeO_2$ spots due to their local thermal reduction to FeO. However, a closer look reveals that all "edge" spots have already disappeared at this point, clearly indicating preferential desorption from the islands edges that dominates in the initial stage of thermal reduction. During the next heating to 690 K, desorption only starts at the end temperature of the previous heating, *i.e.*, 640 K (Figure 3b). The leading edge basically follows the one observed in this temperature range in the "non-stop heated" TPD spectrum as if the desorption process continued from the surface formed in the previous run. After the sample was heated to 690 K, a small amount of $FeO_2$ spots remains on the islands (Figure 3e), which fully disappear after further heating to 900 K (not shown), ultimately recovering the FeO(111) surface. Therefore, STM results show that $O_2$ desorption starts within the $FeO_2$ spots at the island edge and then takes place randomly in the island interior.

In principle, the observed random desorption favors the mechanism of thermal reduction *via* $O_2$ desorption from oxide directly into the gas phase rather than *via* spillover of the O atoms onto the Pt surface from which they desorb associatively. Indeed, the desorption peak obtained for a dense film (*i.e.*, no Pt exposed) has the same shape as the partially covered samples do. In such scenario (desorption into the gas phase), the shift to lower temperatures at decreasing film coverage (Figure 3a) could be interpreted as if oxygen atoms in smaller $FeO_{2-x}$ islands were more weakly bound. In this respect, we note a recent STM study [39] showing that FeO islands below 3 nm in size are more resistant

towards oxidation. This implies that “extra” O species in such small islands are less stable, and, therefore, the islands will more easily release oxygen during heating and thermal reduction. One may argue, that oxide islands studied here (tens of nanometers) are too large for invoking such a strong size effect. If the effect had a purely kinetic origin (larger island needs more time for oxygen desorption, thus causing the peak shifting to higher temperatures), then the TPD spectra would exhibit zero order kinetics with the same leading edge irrespective of the island size, at variance with the experiment. As a hypothesis, we could propose that oxygen desorption is affected by the size-dependent strain in the film as a result of a large (~ 10%) lattice mismatch between the oxide layer and metal surface. Indeed, looking at STM images one may notice that larger islands exhibit roundish and well-ordered $FeO_2$ spots, whereas such spots in the smallest islands as well as at the edge of large islands are considerably distorted.

*Theoretical results*

To get more insight into the oxygen stability in O-rich islands, we have performed DFT calculations on two models: FeO-embedded islands (Figure 4a) and isolated $FeO_2$ islands (Figure 4b). While the former describes the inner part of relatively large islands, the latter corresponds to the smallest, *i.e.*, single-spot island, but may also mimic the edge spots in larger islands.

The embedded model was obtained from the continuous $FeO_2$ tri-layer film by the removal of the most weakly bound oxygen atoms (see Sec. S1 in the Supporting Information, SI), as to preserve large uniform and well-structured tri-layer $FeO_2$ islands in registry with the Pt substrate, and a continuous FeO(111) lattice in between. Since the precise structure of these islands is yet unknown, we have purposely included both zig-zag- and arm-chair-oriented $FeO_2$/FeO boundaries. To allow a direct comparison, the isolated $FeO_2$ islands were constructed with the same stoichiometry, morphology, atomic structure, and position with respect to the substrate as the embedded ones.

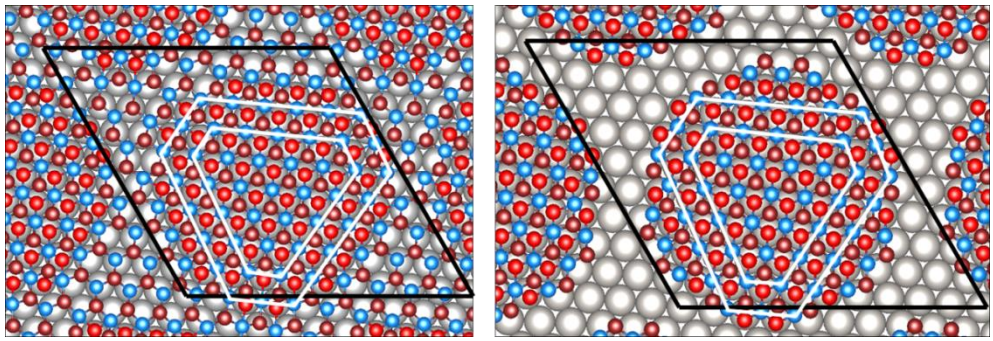

**Figure 4.** Models of FeO-embedded (a) and isolated (b) $FeO_2$ islands on the Pt(111) surface. Pt, Fe, and O atoms are represented by gray, blue, and red (light for interface, dark for surface) spheres, respectively. The peripheric, intermediate, and center zones of the $FeO_2$ islands are delimited (white lines) and the periodic (√73×√73)R5.8°-FeO(111)//(√91×√91)R5.2°-Pt(111) unit cell is indicated (black lines).

In both models, the calculated individual oxygen vacancy formation energies ($\Delta E$) tend to be systematically smaller for interface oxygen atoms and are by far the smallest for interfacial oxygen atoms at the island periphery (Secs. S2 and S3 in SI). This points toward a sequential desorption mode, which starts at the periphery of the $FeO_2$ islands and shifts progressively toward their centers. As a consequence, individual desorption energies are not fully representative of the actual energy cost of island reduction. They also neglect the collective effects in desorption of $O_2$ molecules. To better approximate the desorption thermodynamics, we have simulated the desorption process by the stepwise collective removal of interfacial oxygen atoms successively in the three regions (delimited by white lines in Figure 4), starting from the island periphery. After each desorption stage, the size of the $FeO_2$ region decreases, and the FeO/$FeO_2$ boundary shifts toward the island center.

Table 1 reports the average desorption energies ($\Delta\varepsilon$) at each stage. The lower values of $\Delta\varepsilon$ compared to the average of individual values $\Delta E$ for the atoms upon consideration (Secs. S2 and S3 in SI) highlight the importance of collective effects in the desorption process. Moreover, contrary to an average of all $\Delta E$ values, the average of the three $\Delta\varepsilon$ values reproduces very well the total energy cost (per atom) of a full island reduction (simultaneous removal of all 54 interfacial oxygen atoms in the model), equal to 1.08 eV and 1.01 eV per atom for the embedded and isolated islands, respectively. This difference

corresponds to a nearly 4 eV larger energy cost of the full reduction of the embedded island.

**Table 1.** Average vacancy formation energies $\Delta\varepsilon$ (eV/atom) for the stepwise removal of oxygen atoms in embedded and isolated $FeO_2$ islands. Each successive stage corresponds to the desorption of 18 interfacial oxygen atoms from the peripheric, intermediate, and inner regions, respectively, as shown in Figure 4.

| $\Delta\varepsilon$ (eV/atom) | Stage I (Peripheric) | Stage II (Intermediate) | Stage III (Inner) |
|---|---|---|---|
| Embedded island | 0.95 | 1.13 | 1.15 |
| Isolated island | 0.95 | 1.06 | 0.99 |

Calculated $\Delta\varepsilon$ values show that oxygen stabilities in the two types of island differ quite considerably. While the difference in $\Delta\varepsilon$ is marginal at the first stage I, it becomes significant at the stage II (0.07 eV/atom), and substantial at stage III (0.16 eV/atom). Moreover, for the embedded islands, the increase of $\Delta\varepsilon$ when moving towards the island center suggests a slowdown of oxygen desorption, whereas such effect is not obvious for the isolated islands. The systematically lower oxygen stability in the isolated islands and the enhanced stability of inner oxygen atoms in the embedded ones are qualitatively consistent with the measured lower oxygen desorption temperature from smaller islands and to the observed greater facility to desorb oxygen atoms from the edges of large islands. This finding may also explain the *in situ* STM results (Figure 1), showing considerable increase of the time required for CO to reduce $FeO_2$ domains during the propagation of the reaction towards the island center.

To rationalize the origin of the differences between $\Delta\varepsilon$ values for the isolated and embedded islands, we compared the evolution of their structural characteristics as a function of island size. Synthetic, spatially-resolved information on the oxide structure is provided by the average Fe-Fe distances around cations along the unit cell long diagonal

(see Figure 4). Figure 5 shows that, while the initial Fe-Fe distances in the embedded and isolated $FeO_2$ islands display similarities (compare black lines), their behavior upon progressive oxygen desorption differs significantly, thus suggesting that strain release effects play a role in the different oxygen stability in the two types of islands.

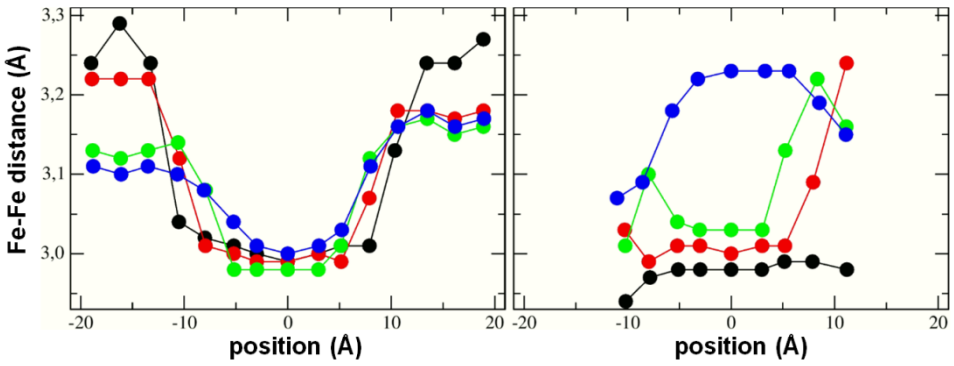


**Figure 5.** Local average values of Fe-Fe distances (Å) for cations along the cell long diagonal for the embedded (left) and isolated (right) islands: initial $FeO_2$ (black); with peripheric O atoms desorbed (red); with peripheric and intermediate O atoms desorbed (green); and fully reduced FeO (blue) islands. (For atomic representations of islands at the various stages of reduction see Figure S6 in SI.)

In the embedded case, the Fe-Fe distances in the interior of the $FeO_2$ islands are nearly size independent and only slightly differ from those in the pristine FeO film in the same region of the Moiré cell. Thus, the embedded O-rich region is not subject to a substantial strain release upon oxygen desorption. However, the structure of the FeO film between the $FeO_2$ islands undergoes important modifications. Indeed, short in-plane lattice parameters of $FeO_2$, consistent with a strong oxide-metal interaction and a large rumpling in the O-Fe-O trilayer film, induce a tensile strain in the inter-island FeO layer. This strain is particularly strong around the full $FeO_2$ islands (black lines in Figure 5), where it produces the largest expansion of the Fe-Fe distances in the FeO zone with respect to those in the corresponding pristine FeO layer (blue). Unsurprisingly, the effect diminishes upon removal of peripheric O atoms (red) and becomes quasi-negligible in the smallest embedded islands (green). In order to estimate the consequence of such strain release on oxygen desorption, in a separate calculation we have released the strain of the FeO region by removing four oxygen atoms from its center. We found that it results in an

increase of $\Delta\varepsilon$ at the stage I by as much as 0.1 eV/atom (Sec. S3 in SI). We thus conclude that the strong tensile strain in the embedding FeO regions substantially reduces the binding of the peripheric O atoms and somewhat weakens the binding of the intermediate ones. It, therefore, explains the progressive increase of $\Delta\varepsilon$ at the subsequent stages of oxygen desorption from the embedded $FeO_2$ islands (Table 1).

In the isolated island, the Fe-Fe distances in the full $FeO_2$ islands (black), are fairly similar to those in the embedded one, suggesting that $d_{Fe\text{-}Fe} \approx 3.0$ Å represents the in-plane lattice parameter in the $FeO_2$/Pt(111) nano-oxide. However, in stark contrast with the embedded case, these distances are much shorter than those in the corresponding fully reduced island (blue). As a consequence, at the successive stages of oxygen desorption, the progressive increase of size of the FeO boundary induces a progressive expansion of the Fe-Fe distances within the remaining $FeO_2$ region. Such behavior indicates the presence of a tensile strain in the $FeO_2$ region, induced by the FeO border. The effect is clearly the most pronounced at the stage III of desorption, at which the departure of oxygen atoms additionally enables a thorough relaxation of the entire FeO island which is additionally accompanied by a change of its registry with respect to the Pt(111) surface. In direct analogy with the embedded case, the presence of such FeO-induced tensile strain reduces the strength of oxygen binding in the $FeO_2$ region, is responsible for the systematically lower $\Delta\varepsilon$ values in the isolated case, and explains the significant reduction of $\Delta\varepsilon$ for the inner oxygen atoms.

To summarize, calculations reveal the specific character of the $FeO_2$/FeO boundary: a large stability difference between surface and interface oxygen atoms and a substantial binding reduction of the latter. As a consequence, oxygen desorption is likely a sequential process triggered by oxygen binding reduction at the progressing $FeO_2$/FeO boundary. Moreover, while different ion coordination and Fe-O bond iono-covalency contribute to the stability of boundary oxygen atoms, we show that strain also plays a prominent role. Indeed, the non-negligible difference of in-plane lattice parameters in the oxygen-rich and oxygen-poor regions affects the oxygen stability at the edges of the embedded islands *via* a strong tensile strain in the inter-island FeO region. Conversely, the tensile strain

induced by the reduced border is the robust cause of oxygen destabilization in the isolated island.

These computational results are consistent with the size effect observed experimentally and clearly show that the thermodynamic stability of oxygen in the $FeO_2$ nano-oxide is sensitive to both its direct environment and to the size of the oxygen-rich phase. However, a translation of the calculated desorption energies $\Delta\varepsilon$ into desorption temperatures using a Redhead analysis as in Ref. [19] leads to differences between embedded and isolated islands roughly twice smaller than those measured experimentally. Several effects of different nature may contribute to such an underestimation. On the one hand, regarding the thermodynamics of desorption, the computational models remain somewhat arbitrary. In particular, while the actual state of the embedding inter-island FeO region under desorption conditions is unknown, we have shown that its strain state significantly affects oxygen stability at the $FeO/FeO_2$ boundary. Interestingly, the roughness of the FeO layer directly after oxygen desorption visible in the STM images (Figure 1) points toward a partial release of the tensile strain in the embedding film. According to our theoretical analysis, this should produce an additional stabilization of oxygen at boundaries of embedded islands, and thus bring the theoretical estimation closer to the measurements. On the other hand, regarding kinetics of oxygen desorption from the boundaries, it may involve activation barriers which do not scale linearly with energy of oxygen desorption, as assumed in Ref.[19] An explicit account for energy barriers associated with alternative oxygen recombination and desorption pathways would be necessary to refine the present thermodynamics-driven estimation.

## 4. Conclusions

Our experimental results show that the CO oxidation reaction on FeO monolayer islands supported by Pt(111) primarily occurs on $FeO/FeO_2$ interface formed under reaction conditions along the islands edge which can be considered as a dynamically fluctuating “reaction zone”. Its width (~ 3 nm) is comparable with the size of a Moiré unit

cell in epitaxial FeO(111)/Pt(111) films thus suggesting the peculiar reactivity of the oxide in the “edge” zone, whereas well-ordered interior regions are relatively inert. As a result, reactivity strongly depends on island size. The islands only consisting of the edge reaction zone show considerably lower (by about 200 K) $CO_2$ formation temperature than the extended islands.

In an attempt to rationalize this effect, we performed oxygen desorption experiments and combined them with an extended DFT analysis to provide insight into the bonding of various oxygen species in such systems since O binding energy has been found as a good descriptor for this reaction on the dense monolayer oxide films. The theoretical results on isolated $FeO_2$ islands indicate a substantially lower stability of the boundary oxygen atoms as compared with the same islands embedded into an FeO layer in qualitative agreement with TPD results showing that the smaller the island, the lower the oxygen desorption temperature.

Size effects are well documented in catalysis over highly dispersed metals in structure sensitive reactions, which are commonly rationalized in terms of abundance of under-coordinated surface atoms on smaller particles considered as the most active sites. Herein, the effect is observed on the *two-dimensional* system.

It should be mentioned that TMO deposits on metal substrates have been long considered as model “inverse” catalysts [40] for studying chemical reactions at the interface between the metal particle and oxide support in “conventional” metal-on-oxide catalysts. Since TMO deposits often form monolayer islands rather than spherical particles,[41] the coverage effects reported for “inverse” model catalysts may be affected by the island size and even cause some discrepancy, if the islands size is not controlled or directly measured.

**Acknowledgements**

The work was supported by Fonds der Chemischen Industrie. K.Z. acknowledges financial support from the NFFA-Europe Project (Grant 654360).

## References

[1] R.K. Grasselli, Selective Oxidation and Ammoxidation Catalysis: Mechanism and Commercial Practice, in: J.P. Bonnelle, B. Delmon, E. Derouane (Eds.) Surface Properties and Catalysis by Non-Metals, Springer Netherlands, Dordrecht, 1983, pp. 289-304.
[2] R.K. Grasselli, Fundamental Principles of Selective Heterogeneous Oxidation Catalysis, Topics in Catalysis, 21 (2002) 79-88.
[3] A. Bielański, J. Haber, Oxygen in Catalysis on Transition Metal Oxides, Catalysis Reviews, 19 (1979) 1-41.
[4] J. Haber, M. Witko, Oxidation catalysis—electronic theory revisited, Journal of Catalysis, 216 (2003) 416-424.
[5] J. Haber, Catalytic Oxidation -State of The Art and Prospects, in: P. Ruiz, B. Delmon (Eds.) Studies in Surface Science and Catalysis, Elsevier, 1992, pp. 279-304.
[6] S.J. Tauster, Strong metal-support interactions, Accounts of Chemical Research, 20 (1987) 389-394.
[7] F. Solymosi, Importance of the Electric Properties of Supports in the Carrier Effect, Catalysis Reviews, 1 (1968) 233-255.
[8] G.L. Haller, D.E. Resasco, Metal–Support Interaction: Group VIII Metals and Reducible Oxides, in: H.P. D.D. Eley, B.W. Paul (Eds.) Adv. Catal., Academic Press, 1989, pp. 173-235.
[9] S. Bernal, J.J. Calvino, M.A. Cauqui, J.M. Gatica, C. Larese, J.A. Pérez Omil, J.M. Pintado, Some recent results on metal/support interaction effects in NM/CeO2 (NM: noble metal) catalysts, Catalysis Today, 50 (1999) 175-206.
[10] F.F. Vol'kenshtein, Experiment and the electronic theory of catalysis, Russian Chemical Reviews, 35 (1966) 537.
[11] S. Shaikhutdinov, Strong Metal–Support Interaction and Reactivity of Ultrathin Oxide Films, Catalysis Letters, 148 (2018) 2627-2635.
[12] Y.-N. Sun, L. Giordano, J. Goniakowski, M. Lewandowski, Z.-H. Qin, C. Noguera, S. Shaikhutdinov, G. Pacchioni, H.-J. Freund, The Interplay between Structure and CO Oxidation Catalysis on Metal-Supported Ultrathin Oxide Films, Angewandte Chemie International Edition, 49 (2010) 4418-4421.
[13] Z.H. Qin, M. Lewandowski, Y.N. Sun, S. Shaikhutdinov, H.J. Freund, Encapsulation of Pt Nanoparticles as a Result of Strong Metal−Support Interaction with Fe3O4(111), The Journal of Physical Chemistry C, 112 (2008) 10209-10213.
[14] M.G. Willinger, W. Zhang, O. Bondarchuk, S. Shaikhutdinov, H.-J. Freund, R. Schlögl, A Case of Strong Metal–Support Interactions: Combining Advanced Microscopy and Model Systems to Elucidate the Atomic Structure of Interfaces, Angewandte Chemie International Edition, 53 (2014) 5998-6001.
[15] G.H. Vurens, V. Maurice, M. Salmeron, G.A. Somorjai, Growth, structure and chemical properties of FeO overlayers on Pt(100) and Pt(111), Surface Science, 268 (1992) 170-178.
[16] L. Giordano, M. Lewandowski, I.M.N. Groot, Y.N. Sun, J. Goniakowski, C. Noguera, S. Shaikhutdinov, G. Pacchioni, H.J. Freund, Oxygen-Induced Transformations of an FeO(111) Film on Pt(111): A Combined DFT and STM Study, Journal of Physical Chemistry C, 114 (2010) 21504-21509.
[17] L.R. Merte, Y. Bai, H. Zeuthen, G. Peng, L. Lammich, F. Besenbacher, M. Mavrikakis, S. Wendt, Identification of O-rich structures on platinum(111)-supported ultrathin iron oxide films, Surface Science, 652 (2016) 261-268.

[18] Y. Martynova, S. Shaikhutdinov, H.-J. Freund, CO Oxidation on Metal-Supported Ultrathin Oxide Films: What Makes Them Active?, Chemcatchem, 5 (2013) 2162-2166.
[19] Q. Pan, X. Weng, M. Chen, L. Giordano, G. Pacchioni, C. Noguera, J. Goniakowski, S. Shaikhutdinov, H.-J. Freund, Enhanced CO Oxidation on the Oxide/Metal Interface: From Ultra-High Vacuum to Near-Atmospheric Pressures, ChemCatChem, 7 (2015) 2620-2627.
[20] Y. Martynova, B.H. Liu, M.E. McBriarty, I.M.N. Groot, M.J. Bedzyk, S. Shaikhutdinov, H.J. Freund, CO oxidation over ZnO films on Pt(111) at near-atmospheric pressures, Journal of Catalysis, 301 (2013) 227-232.
[21] D. Sun, X.-K. Gu, R. Ouyang, H.-Y. Su, Q. Fu, X. Bao, W.-X. Li, Theoretical Study of the Role of a Metal–Cation Ensemble at the Oxide–Metal Boundary on CO Oxidation, The Journal of Physical Chemistry C, 116 (2012) 7491-7498.
[22] K. Zhang, L. Li, S. Shaikhutdinov, H.-J. Freund, Carbon Monoxide Oxidation on Metal-Supported Monolayer Oxide Films: Establishing Which Interface is Active, Angewandte Chemie International Edition, 57 (2018) 1261-1265.
[23] G. Kresse, J. Furthmüller, Efficient iterative schemes for ab initio total-energy calculations using a plane-wave basis set, Physical Review B, 54 (1996) 11169-11186.
[24] G. Kresse, J. Hafner, Ab initio molecular-dynamics simulation of the liquid-metal--amorphous-semiconductor transition in germanium, Physical Review B, 49 (1994) 14251-14269.
[25] G. Kresse, D. Joubert, From ultrasoft pseudopotentials to the projector augmented-wave method, Physical Review B, 59 (1999) 1758-1775.
[26] P.E. Blöchl, Projector augmented-wave method, Physical Review B, 50 (1994) 17953-17979.
[27] J.P. Perdew, J.A. Chevary, S.H. Vosko, K.A. Jackson, M.R. Pederson, D.J. Singh, C. Fiolhais, Atoms, molecules, solids, and surfaces: Applications of the generalized gradient approximation for exchange and correlation, Physical Review B, 46 (1992) 6671-6687.
[28] L. Giordano, G. Pacchioni, J. Goniakowski, N. Nilius, E.D.L. Rienks, H.-J. Freund, Interplay between structural, magnetic, and electronic properties in a FeO/Pt(111) ultrathin film, Physical Review B, 76 (2007) 075416.
[29] S. Prada, L. Giordano, G. Pacchioni, C. Noguera, J. Goniakowski, Properties of Pt-supported iron oxide ultra-thin films: Similarity of Hubbard-corrected and hybrid density functional theory description, The Journal of Chemical Physics, 141 (2014) 144702.
[30] S.L. Dudarev, G.A. Botton, S.Y. Savrasov, C.J. Humphreys, A.P. Sutton, Electron-energy-loss spectra and the structural stability of nickel oxide: An LSDA+U study, Physical Review B, 57 (1998) 1505-1509.
[31] M. Ritter, W. Ranke, W. Weiss, Growth and structure of ultrathin FeO films on Pt(111) studied by STM and LEED, Physical Review B, 57 (1998) 7240-7251.
[32] L. Giordano, G. Pacchioni, C. Noguera, J. Goniakowski, Identification of Active Sites in a Realistic Model of Strong Metal–Support Interaction Catalysts: The Case of Platinum (1 1 1)-Supported Iron Oxide Film, ChemCatChem, 6 (2014) 185-190.
[33] R.F.W. Bader, A quantum theory of molecular structure and its applications, Chemical Reviews, 91 (1991) 893-928.
[34] G. Henkelman, A. Arnaldsson, H. Jónsson, A fast and robust algorithm for Bader decomposition of charge density, Computational Materials Science, 36 (2006) 354-360.
[35] K. Momma, F. Izumi, VESTA 3 for three-dimensional visualization of crystal, volumetric and morphology data, Journal of Applied Crystallography, 44 (2011) 1272-1276.
[36] N.A. Saliba, Y.L. Tsai, C. Panja, B.E. Koel, Oxidation of Pt(111) by ozone (O3) under UHV conditions, Surface Science, 419 (1999) 79-88.
[37] J.F. Weaver, J.-J. Chen, A.L. Gerrard, Oxidation of Pt(111) by gas-phase oxygen atoms, Surface Science, 592 (2005) 83-103.

[38] B. Klötzer, K. Hayek, C. Konvicka, E. Lundgren, P. Varga, Oxygen-induced surface phase transformation of Pd(111): sticking, adsorption and desorption kinetics, Surface Science, 482-485 (2001) 237-242.
[39] Y. Liu, F. Yang, Y. Zhang, J. Xiao, L. Yu, Q. Liu, Y. Ning, Z. Zhou, H. Chen, W. Huang, P. Liu, X. Bao, Enhanced oxidation resistance of active nanostructures via dynamic size effect, Nature Communications, 8 (2017) 14459.
[40] K. Hayek, B. Jenewein, B. Klötzer, W. Reichl, Surface reactions on inverse model catalysts: CO adsorption and CO hydrogenation on vanadia- and ceria-modified surfaces of rhodium and palladium, Topics in Catalysis, 14 (2000) 25-33.
[41] F.P. Netzer, F. Allegretti, S. Surnev, Low-dimensional oxide nanostructures on metals: Hybrid systems with novel properties, Journal of Vacuum Science & Technology B: Microelectronics and Nanometer Structures, 28 (2010) 1-16.

**SUPPORTING INFORMATION for:**

# Size effect in two-dimensional oxide-on-metal catalysts of CO oxidation and its connection to oxygen bonding: An experimental and theoretical approach

Ke Zhang, Linfei Li, Jacek Goniakowski,* Claudine Noguera

Hans-Joachim Freund, Shamil Shaikhutdinov*

The supporting information provides a detailed description of the results obtained from the DFT simulations of a continuous $FeO_2$ film (Section S1), of FeO-embedded $FeO_2$ islands (Section S2), and of isolated $FeO_2$ islands (Section S3).

## S1. Structural, electronic, and stability characteristics of the continuous Pt(111)-supported $FeO_2$ film.

To get an insight into the characteristics of the oxygen-rich iron oxide which forms on the Pt(111) surface upon exposition of an FeO(111) layer to oxygen, we have performed DFT calculations on a continuous $FeO_2$ film obtained by a thorough structural relaxation of the initial (√73×√73)R5.8° -FeO(111) // (√91×√91)R5.2° -Pt(111) layer fully covered with oxygen adatoms (one ad-oxygen per FeO formula unit). The resulting atomic structure of the oxide film is shown in Fig. S1 and its key structural and electronic characteristics are summarized in Fig S2.

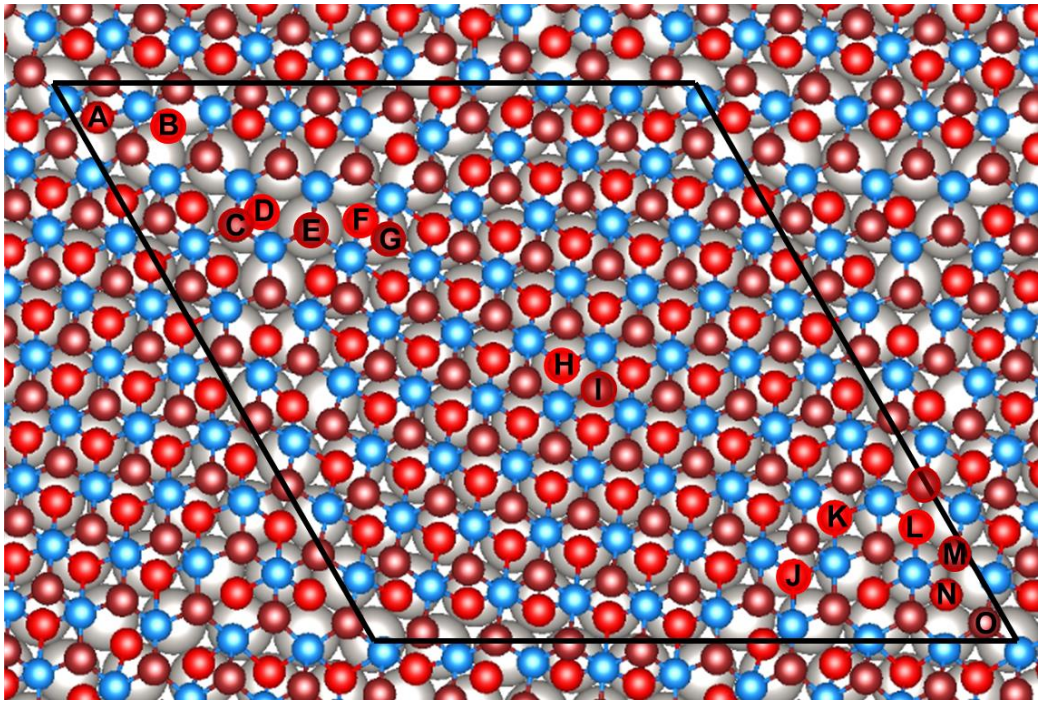


**Figure S1.** Model of the Pt(111) surface fully covered with a $FeO_2$ oxide film. Selected oxygen sites in different regions of the Moiré cell are labeled A-O. Pt, Fe, and O atoms are represented by gray, blue, and red (light for interface, dark for surface) spheres, respectively. The periodic unit cell is indicated.

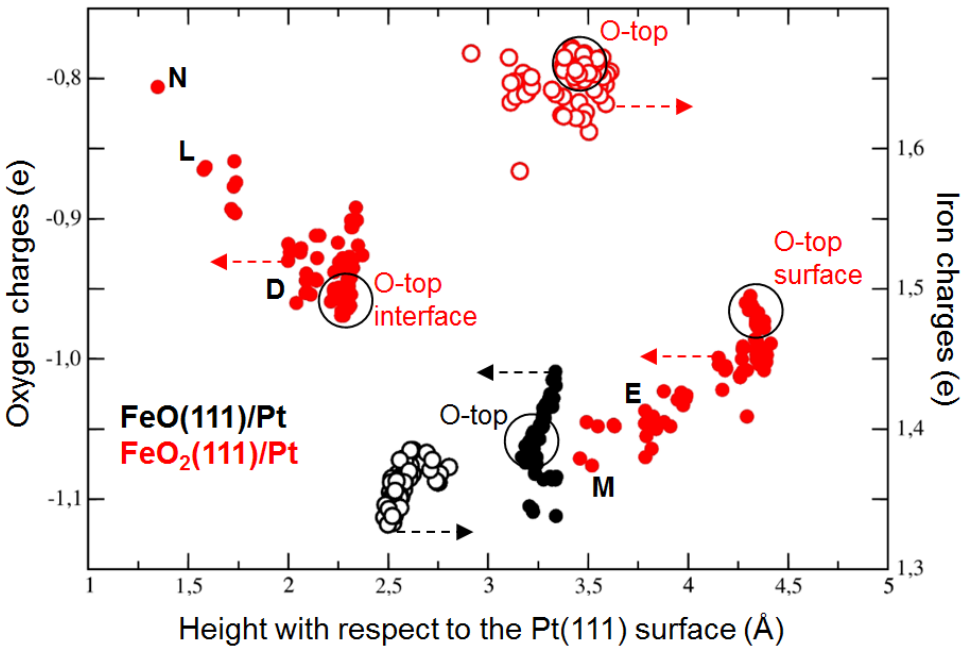


**Figure S2:** Key structural (distance from the Pt substrate) and electronic (Bader charges) characteristics of anions (full circles) and cations (empty circles) in the $FeO_2$ (red) and FeO (black) films. Surface and interface oxygen atoms are located at a height larger and smaller than c.a. 2.5 Å from the Pt(111) surface, respectively.

Oxygen adatoms provoke a profound restructuration of the initial FeO layer. All Fe cations move away from the Pt surface and their Bader charges substantially increase. Oxygen atoms split into two distinct groups: the interfacial and the surface ones, positioned close to (< 2.5 Å) and further away (> 2.5 Å) from the Pt surface, respectively. Regardless their position, Bader charges of most oxygen atoms are only little reduced compared to those in the initial FeO film, which shows a full accommodation of all oxygen ad-atoms in the oxide film, with the formal $O^{2-}$ oxidation state. The unusual $FeO_2$ film stoichiometry with formally $Fe^{3+}$ cations is enabled by a substantial electron transfer from the Pt(111) substrate towards the oxide film (0.3e/$FeO_2$, as opposed to -0.3e/FeO in the initial FeO layer), which confers to the oxygen-rich iron oxide film a specific nano-oxide character.

The structural and electronic characteristics of the supported $FeO_2$ film strongly depend on the local registry between the film lattice and the underlying Pt(111) surface. A regular and homogeneous O-Fe-O trilayer structure, characteristic of the largest part of the Moiré cell, is associated with interface anions located on top of surface Pt atoms (large vicinity of sites H and I in Fig. S1 and sites labeled "O-top" in Fig. S2). Conversely, when interface anions are located in surface hollow or bridge sites they move closer to the Pt surface, such that the trilayer structure is partially broken. This is best exemplified by oxygen atoms in sites A, B, D, F, L, and N, which form less than three O-Fe bonds with the oxide film. In these small regions of the Moiré cell, also the surface anions tend to move inward (e.g., sites E, M, and O) such that the structure of the FeO layer is partially recovered. However, the presence of interfacial oxygen atoms makes this FeO-like film more distant from the Pt substrate, and maintains the cation $Fe^{3+}$ -like oxidation state of cations. The strong structural modulation of the $FeO_2$ film with the particularly large height of surface oxygens in the O-top regions only is consistent with the experimental STM signature of the oxygen-rich film, characterized by a single large region of enhanced contrast per Moiré cell.

Regarding the thermodynamic stability of oxygen atoms in the supported $FeO_2$ film, individual desorption energies in different regions of the Moiré cell, Table S1, display a particularly wide span of values, ranging from 0.2 to 1.6 eV. The regular $FeO_2$ trilayer structure in the large O-top region is characterized by the strongest bonding of its oxygen atoms (sites H and I). It is only somewhat reduced when moving toward region boundaries (site G). Conversely, oxygen atoms in the small Fe-top region are the least stable (smallest desorption energies at sites L, M, N, O). We note that the desorption of a surface oxygen from this region (sites M, O) provokes a spontaneous substitution of the vacancy by an interfacial one (L, N), thus recovering the regular FeO layer structure with 3-fold coordinated ions. Finally, the medium-size region in which both interface oxygens and cations are located in surface hollow sites (sites C, D, E, and F) is characterized by an intermediate oxygen bonding. Interestingly, the removal of a

surface oxygen from this region (sites C, E) locally breaks the film structure due to an important outward relaxation of the surrounding ions. It thus witnesses the presence of an important tensile strain in the oxide film which is released upon oxygen desorption (see Section S3).

| | L, M, N, O | C, E | D, J, K | A, B, F | G | H, I |
|---|---|---|---|---|---|---|
| $\Delta$E | 0.2 | 0.7-0.8 | 0.9 | 1.0 | 1.4 | 1.6 |

**Table S1.** Desorption energies $\Delta$E (eV) of individual oxygen atoms from different regions of the continuous $FeO_2$ film, Fig. S1. Larger oxygen stability is associated to larger $\Delta$E values.

## S2. Oxygen stability in the FeO-embedded $FeO_2$ islands.

In the following we focus on the properties of large well-structured $FeO_2$ islands which form in regions in which interface anions are located on top of surface Pt atoms. As shown in Sec. S1, the oxygen-rich oxide film displays in these regions a regular and uniform O-Fe-O trilayer structure and is characterized by the strongest binding of both its surface and interfacial anions (the largest desorption energies $\Delta$E of individual oxygen atoms, Tab. S1). To this goal we have removed the most weakly bound interfacial oxygen atoms from the continuous $FeO_2$ film, as to preserve the large and well-structured trilayer $FeO_2$ islands in the O-top regions and a continuous FeO(111) lattice in the inter-island regions, Fig. S3. Since the precise morphology and atomic structure of such embedded oxygen-rich islands are unknown, we have purposely included both zig-zag- and arm-chair-oriented $FeO_2$/FeO boundaries. All inequivalent oxygen sites in the irreducible part of the $FeO_2$ island are labeled a-v.

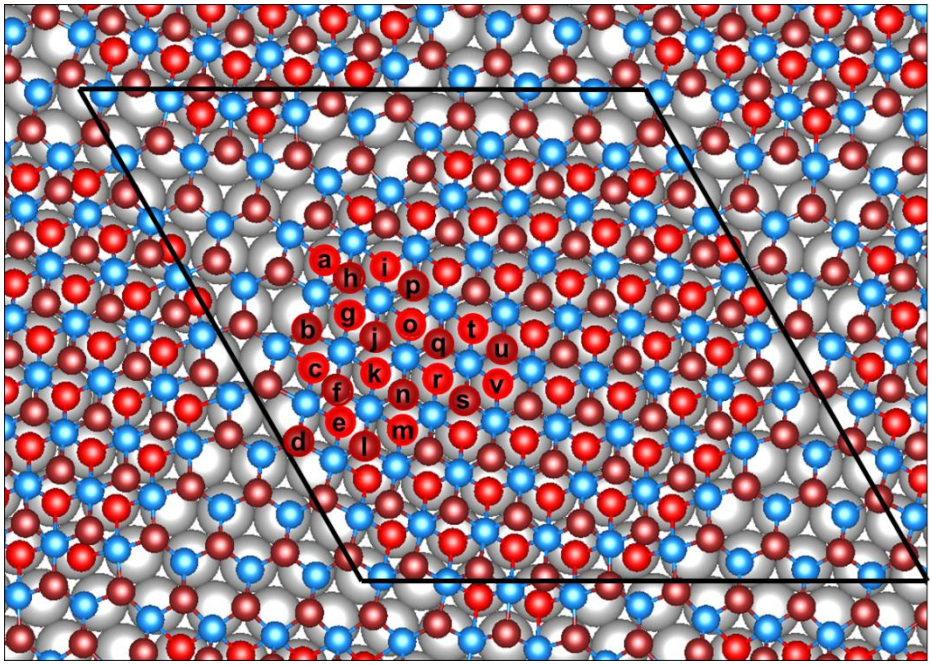


**Figure S3.** Model of a $FeO_2$ island embedded in the FeO(111) layer on the Pt(111) surface. Inequivalent oxygen sites are labeled a–v. Pt, Fe, and O atoms are represented by gray, blue, and red (light for interface, dark for surface) spheres, respectively. The periodic unit cell is indicated.

Table S2 shows a relatively strong site dependence of the calculated vacancy formation energies $\Delta E$ (0.9 eV < $\Delta E$ < 3.3 eV). Surface and interface oxygen atoms in the very island center (sites s, t, u, v) display fairly similar large stabilities ($\Delta E$ = 1.5 - 1.7 eV), which are close to those found for the same sites in the continuous $FeO_2$ film, Sec S1. However, when moving from island center toward its boundaries, surface oxygen atoms become more strongly bound ($\Delta E$ = 1.8 – 2.1 eV) than those at the interface ($\Delta E$ = 1.4 - 1.5 eV). The difference between the two types of atoms becomes paramount at the very $FeO_2$/FeO boundary where surface sites with $\Delta E$ of about 3 eV (sites b, d), characteristic of a pristine 1ML-FeO(111)/Pt(111), coexist with interface sites with $\Delta E$ smaller than 1 eV (sites a and c), characteristic of some less well-structured inter-island regions of the continuous $FeO_2$ film, Sec. S1.

| Type | interface | | | surface | | |
|---|---|---|---|---|---|---|
| Site label | a, c | g, k, i, m, o, r | e, t, v | f, h, l, s, u | j, n, p, q | b, d |
| $\Delta$E (eV) | 0.9 | 1.4 - 1.5 | 1.5 - 1.6 | 1.6 - 1.7 | 1.8 - 2.1 | 2.4 - 3.3 |

**Table S2.** Calculated vacancy formation energies $\Delta$E (eV) for individual surface and interfacial oxygen atoms in FeO-embedded $FeO_2$ islands on the Pt(111) surface. Site labels a-v refer to those marked in Fig. S3.

These results reveal the specific character of the very $FeO_2$/FeO boundary for the oxygen stability. On the one hand, since the interfacial atoms at the boundary become by far the most prompt to desorption, the remaining strongly bound surface atoms will assure the continuity of the FeO(111) lattice, thus facilitating the reversibility of oxygen uptake and release by the embedded $FeO_2$ islands. More importantly, the particularly small $\Delta$E values of interfacial boundary sites ($\Delta$E = 0.9 eV, compared to 1.6 eV in the island center) show that any temperature programmed oxygen desorption will start there. Interestingly, we find that since the removal of these weakly bound oxygen atoms (sites a and c and all equivalent by symmetry) shifts the $FeO_2$/FeO boundary towards the island interior, it simultaneously lowers the binding of interfacial oxygen atoms at the newly exposed $FeO_2$/FeO boundary (sites g, e, and i) compared to the corresponding $\Delta$E values in Tab. S2 (by -0.3 eV, -0.2 eV, and -0.1 eV, respectively). These finding points toward a sequential mode of oxygen desorption from the embedded $FeO_2$ islands, which involves a removal of interfacial oxygen at the $FeO_2$/FeO boundary, accompanied by a progressive boundary shift towards the island center.

Such sequential oxygen desorption triggered by $\Delta$E reduction at the progressing $FeO_2$/FeO boundary makes the individual vacancy formation energies, Tab. S2, not fully representative of the actual energy cost of island reduction. Indeed, an average of $\Delta$E from Table S1 (1.34 eV/atom) is noticeably larger than that calculated for a

simultaneous desorption of all interfacial oxygen atoms (1.08 eV/atom). Moreover, since $\Delta$E values clearly depend on the local environment of the oxygen atoms, a co-operative desorption of anions (e.g., of two neighboring anions, as to form an $O_2$ molecule) differs from a sum of individual vacancy formation energies. For exemple, we find that a simultaneous removal of two atoms from neighboring sites a requires 0.75 eV/atom, much less than 0.9 eV/atom found for the individual desorption, Tab. S2.

As to better account for these collective and co-operative effects on the thermodynamics of oxygen desorption in the embedded $FeO_2$ islands, we have mimicked the actual desorption process by the removal of interfacial boundary oxygen atoms in three stages, Tab S3. The first stage consists of a simultaneous removal of all interfacial oxygen atoms at the initial $FeO_2$/FeO boundary (sites a, c, e, and all equivalent by symmetry) and is characterized by the corresponding average oxygen vacancy formation energy $\Delta\varepsilon$. Further on, the subsequent interfacial atoms are simultaneously removed from the newly formed boundary (sites g, k, I, m, and all equivalent by symmetry) at the second stage. Finally, the remaining interfacial atoms (sites o, r, t, v, and all equivalent by symmetry) are simultaneously removed at stage III.

| Desorption stage | Stage I | Stage II | Stage III |
|---|---|---|---|
| Site labels | a, c, e | g, k, I, m | o, r, t, v |
| $\Delta\varepsilon$ (eV/atom) | 0.95 | 1.13 | 1.15 |

**Table S3.** Calculated average vacancy formation energies $\Delta\varepsilon$ (eV/atom) for the simultaneous removal of interfacial oxygen atoms from the $FeO_2$/FeO boundary in FeO-embedded $FeO_2$ islands on the Pt(111) surface. The three stages correspond to three successive locations of the boundary in the island. The labels of the removed oxygen atoms (a total of 18 atoms at each stage) refer to those marked in Fig. S3.

Table S3 shows that the collective desorption energies of boundary interfacial oxygen atoms $\Delta\varepsilon$ are indeed systematically smaller than the corresponding averages of individual desorption energies $\Delta E$, Tab. S2, and fully confirm the specific role of $FeO_2$/FeO boundary for the ease of oxygen desorption. Unsurprisingly, the most important difference concerns the island center (stage III), where $\Delta\varepsilon$ = 1.15 eV is by as much as 0.4-0.5 eV/atom smaller than individual values $\Delta E$ = 1.5 - 1.6 eV. The effect is also quite substantial (-0.15 eV) for the energetics of the initial island edge (stage I), as already hinted above by the results on co-operative removal of two oxygens from neighboring sites a. It is worth stressing that, contrary to an average of $\Delta E$ values, the average of the three $\Delta\varepsilon$ values reproduces very well the energy cost (per atom) of the full reduction of the embedded island (simultaneous desorption of all 54 interfacial atoms) equal to 1.08 eV/atom. Finally, the present results also reveal an increase of oxygen binding as the $FeO_2$/FeO boundary progresses towards the island center. Indeed, it is the weakest at the boundary of the initial islands (stage I), but increases progressively as the islands become smaller (stage II and III).

## S3. Oxygen stability in isolated $FeO_2$ islands on the Pt(111) surface.

As to estimate the effect of FeO-embedding on the oxygen stability in the $FeO_2$ islands we have performed complementary DFT calculations on isolated $FeO_2$ islands, Fig. S4, of the same stoichiometry, morphology, atomic structure, and position with respect to the substrate as the embedded ones analyzed in Sec. S2. Such objects represent the smallest experimental islands, characterized by a single STM spot only, but may also account for effects at edges of larger islands, where the FeO-embedding is partially absent.

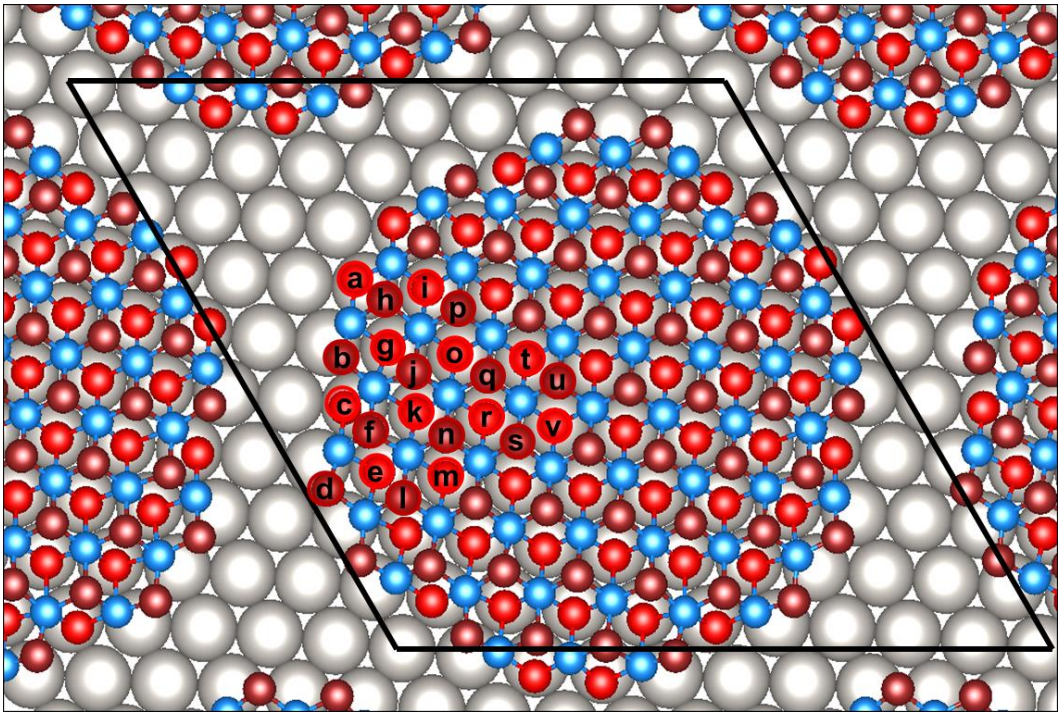


**Figure S4.** Computational model of the an isolated $FeO_2$ island on the Pt(111) surface. Irreducible oxygen sites are labeled a–v, consistently with those in Fig. S3.

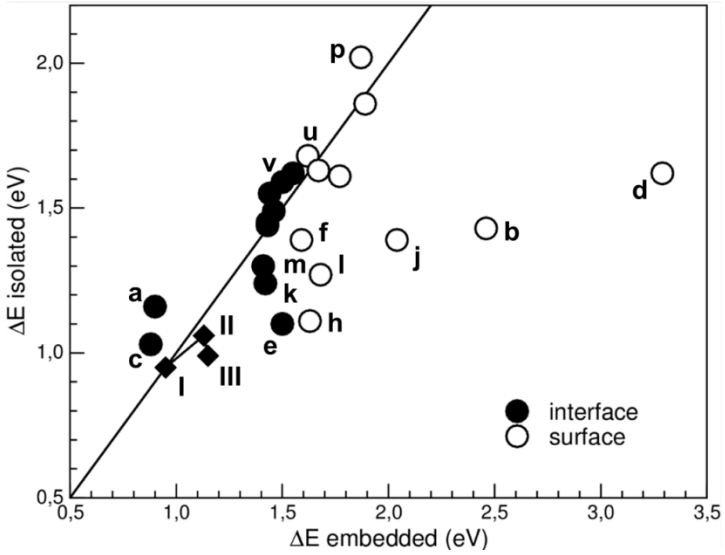


**Figure S5.** Comparison of individual ($\Delta E$) and collective ($\Delta\varepsilon$) oxygen vacancy formation energies for interface (full circles) and surface (open circles) sites a–v, Figs. S3 and S4, and for I-III subsequent desorption stages (full diamonds) in the isolated and embedded $FeO_2$ islands.

The individual $\Delta E$ and average $\Delta\varepsilon$ vacancy formation energies calculated for the isolated island are compared to the corresponding results for the FeO-embedded one in Fig. S5. The individual vacancy formation energies $\Delta E$ of the two types of islands show several quantitative and qualitative similarities. $\Delta E$ values tend to be systematically smaller for interface oxygen atoms and the least stable (weakly bound) oxygen atoms are systematically found at the very island periphery (sites a and c). This shows that the scenario of oxygen desorption triggered by $\Delta E$ reduction at the progressing $FeO_2$/FeO boundary is essentially the same in the isolated and embedded islands. However, Fig. S5 also demonstrates that the stability of several surface and interface sites is substantially lower in the isolated case. This difference principally concerns atoms at and close to the isolated island boundary and is particularly well pronounced for surface sites b and d, which display $\Delta E$ values more than 1 eV lower than in the embedded case. Similarly, binding of surface atoms j, f, l and h and of the interface atoms e, k, and m is by 0.1-0.4 eV smaller. Conversely, in the island interior (sites o-v), there is a slight average increase of $\Delta E$ with respect to the embedded case. Interestingly, this increase also concerns interface sites a and c at the very island periphery. As far as $\Delta\varepsilon$ values are concerned, Fig. S5 evidences that isolated islands systematically require less energy to be reduced. The difference in $\Delta\varepsilon$ is marginal at the first stage (0.95 vs 0.95 eV/atom for isolated and embedded islands, respectively), increases at the second one (1.06 vs 1.13 eV/atom), and becomes paramount at stage III (0.99 vs 1.15 eV/atom). This translates into a 4 eV lower energy cost of the full reduction of the isolated island. Moreover, in the embedded case, the progressive increase of $\Delta\varepsilon$ when moving towards the island center suggests a slowdown of oxygen desorption during island reduction, whereas such effect is absent in the isolated object. The systematically lower average oxygen stability in the isolated islands corresponds well to the measured lower oxygen desorption temperature from smaller islands and to the observed greater facility to desorb oxygen atoms from the edges of large islands.

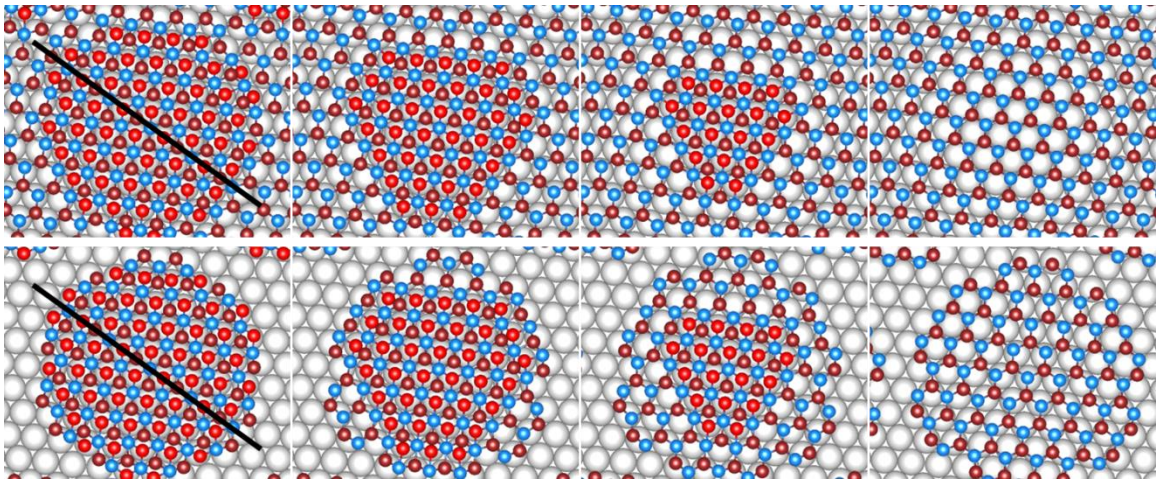

**Figure S6.** Atomic structure of the embedded (top panels) and isolated (bottom panels) $FeO_2$ islands at the three stages of oxygen desorption. From left to right: full, with peripheric oxygen atoms desorbed, with peripheric and intermediate oxygen atoms desorbed, and fully reduced islands. Pt, Fe, and O atoms are represented by gray, blue, and red (light for interface, dark for surface) spheres, respectively.

As to highlight the differences between the isolated and embedded cases, in the following we analyze the electronic (electron exchange with the Pt substrate and oxygen charges) and structural (elastic strain) characteristics of the $FeO_2$ islands, with a special focus on the characteristics of oxygen sites at the island boundaries, and on their evolution as a function of island size. The considered embedded and isolated islands at the three stages of oxygen desorption are depicted in Fig. S6.

We recall that the oxygen-rich $FeO_2$ nano-oxide is mainly stabilized by an electron transfer from the Pt substrate. Indeed, Fig. S7 (top panels) shows that a substantial positive charging of the Pt atoms underlying the $FeO_2$ islands takes place, in contrast to a smaller negative one below the FeO film. Our results clearly show that the effect of positive Pt charging is fairly independent of the island type and size. We note that the Pt charge value in the FeO regions between the full $FeO_2$ embedded islands (black symbols, vicinity of site E, Fig. S7, top left panel) substantially departs from those in the FeO layer. This effect is much smaller and becomes quasi-negligible in smaller embedded islands.

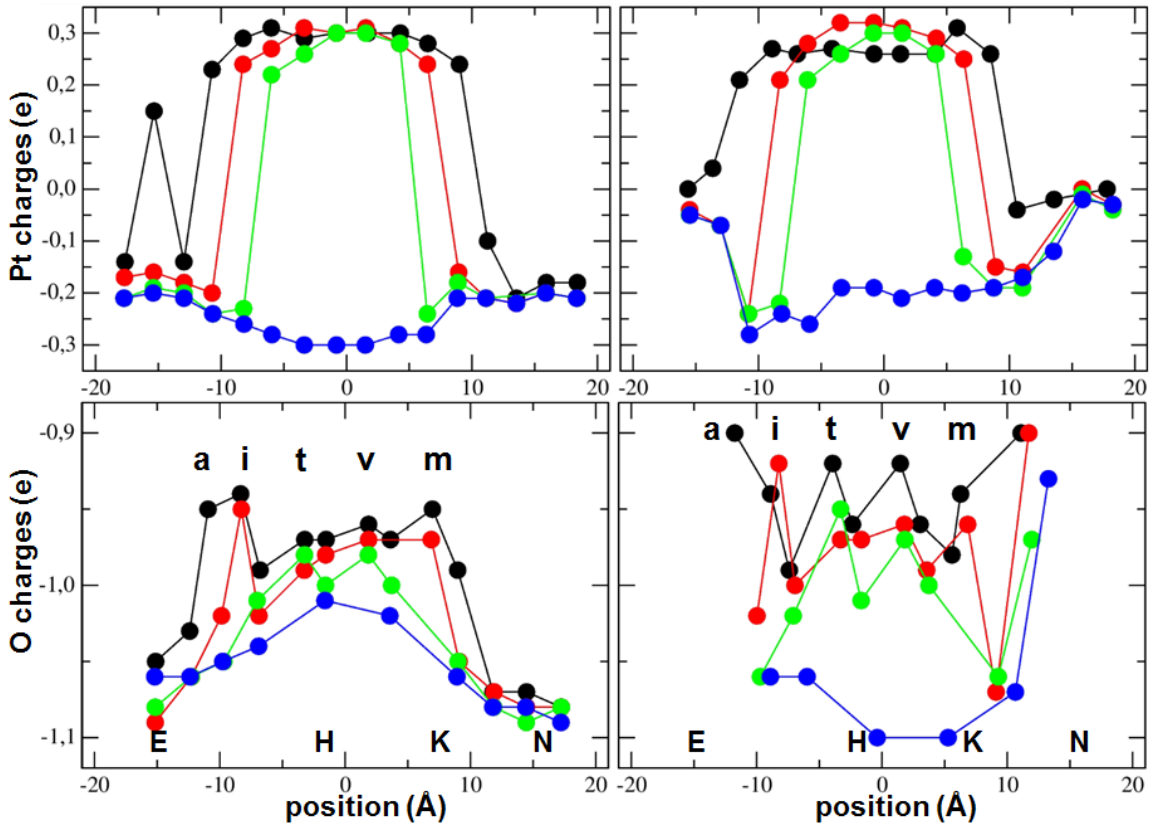


**Figure S7.** Bader charges of surface Pt (top) and oxygen (bottom) atoms, taken along the segments indicated in Fig. S6, for the embedded (left) and isolated (right) islands: full (black), with peripheric oxygen atoms desorbed (red), with peripheric and intermediate oxygen atoms desorbed (green), and fully reduced (blue). Labels E, H, K, and N refer to sites in Fig. S1. Labels a, i, t, v, and m refer to Figs. S3 and S4.

Despite this overall similarity of interface charge transfers, the charges of oxygen atoms in the $FeO_2$ islands display significant differences (Fig. S7, bottom panels). In direct analogy to the $\Delta E$ values, in the embedded islands charges of surface and interface oxygen atoms are roughly alike in the island centers, but the difference between the two types of sites increases when moving towards island boundaries where charges of interfacial atoms are systematically smaller. In the isolated islands the

charge differentiation between the two types of oxygen sites is systematically much more pronounced and is clearly visible also in the island centers. Moreover, boundary charges are systematically smaller in the isolated islands. This effect is particularly striking at the boundary of full islands where low coordinated site a (2 O-Fe bonds in the isolated islands versus 3 in the embedded ones) experiences the most pronounced charge reduction. However, the effect clearly concerns also the fully coordinated boundary sites i and m (second desorption stage) and t and v (third desorption stage), where all oxygen atoms are fully coordinated.

The correlation between the behavior of $Q_O$ and $\Delta E$ values tends to link the origin of oxygen desorption energy variations to differences of number and covalency of the O-Fe bonds at the island boundary. However, Fig. S8 shows that, while the Fe-Fe distances in the full embedded and isolated $FeO_2$ islands (black) display similarities, their behavior upon progressive oxygen desorption differs significantly, thus suggesting that strain release effects play also a role in the different oxygen stability in the two types of islands.

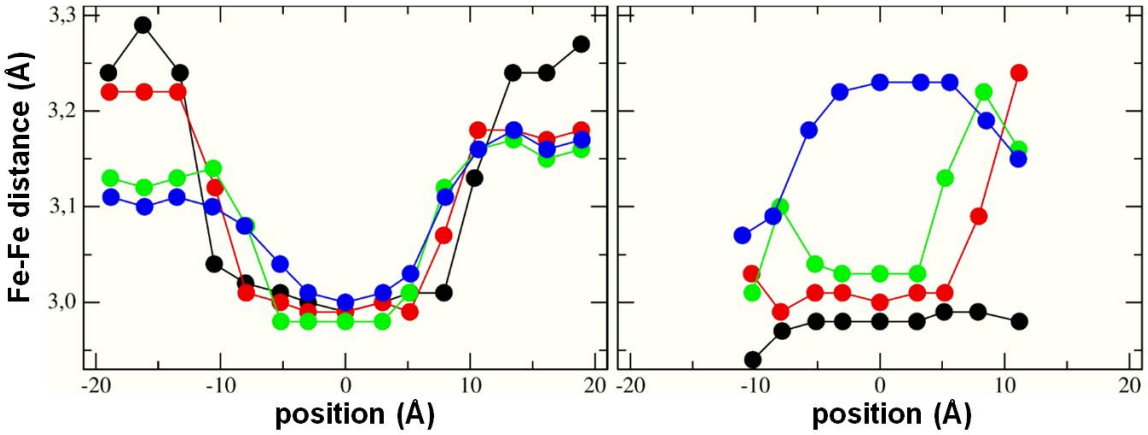


**Figure S8.** Local average values of Fe-Fe distances (Å) for cations along the cell long diagonal for the embedded (left) and isolated (right) islands: full (black), with peripheric oxygen atoms desorbed (red), with peripheric and intermediate oxygen atoms desorbed (green), and fully reduced (blue) islands.

In the embedded case, the Fe-Fe distances in the interior of the $FeO_2$ islands are nearly size independent and differ only very little from those in the pristine FeO film in the same region of the Moiré cell. Thus, the embedded oxygen-rich region is not subject to a substantial strain release upon oxygen desorption. However, Fig. S8 shows that the structure of the FeO film between the $FeO_2$ islands undergoes important modifications. Indeed, short in-plane lattice parameters of $FeO_2$, consistent with a strong oxide-metal interaction and a large rumpling in the trilayer film, induce a tensile strain in the inter-island FeO layer. This strain is particularly strong around the full $FeO_2$ islands (black), where it produces the largest expansion of the Fe-Fe distances in the FeO zone with respect to those in the corresponding pristine FeO layer (blue). Unsurprisingly, this effect diminishes upon removal of peripheric oxygen atoms (red) and becomes quasi-negligible in the smallest embedded islands (green). In order to estimate the consequence of such strain release on oxygen desorption, in a separate calculation we have partially released the strain of the embedding FeO film by removing one and four oxygen atoms from its center, Fig. S9. We found that such removal results in an enhancement of $\Delta$E value of the site a by as much as 0.3 eV (single oxygen atoms removed), and in an increase of $\Delta\varepsilon$ at the first stage by as much as 0.1 eV/atom (four atoms removed). We thus conclude that the strong tensile strain in the embedding FeO regions substantially reduces the binding of the peripheric oxygen atoms and somewhat weakens the binding of the intermediate ones. It thus explains the calculated progressive increase of $\Delta\varepsilon$ at the subsequent stages of oxygen desorption from the embedded $FeO_2$ islands.

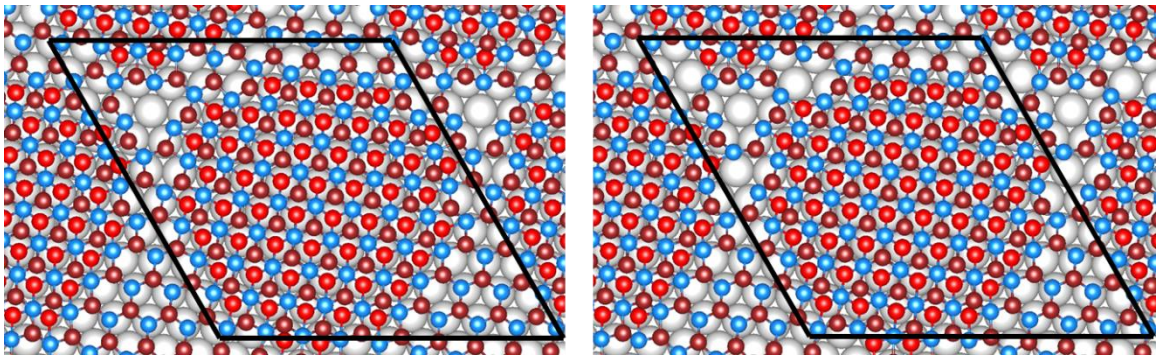

**Figure S9.** Atomic structure of the full embedded $FeO_2$ islands with one (left) and four (right) atoms removed from the strained embedding FeO layer. Large outward relaxation of the surrounding lattice witnesses a substantial strain relief.

In the isolated case, the Fe-Fe distances in the full $FeO_2$ islands (black), are fairly similar to those in the embedded one, suggesting that $d_{Fe\text{-}Fe} \cong 3.0$ Å represents the in-plane lattice parameter of the $FeO_2$/Pt(111) nano-oxide. However, in stark contrast with the embedded case, these distances are much shorter than those in the corresponding fully reduced island (blue). As a consequence, at the successive stages of oxygen desorption, the progressive increase of size of the FeO zone induces a progressive expansion of the Fe-Fe distances within the remaining $FeO_2$ region. Such behavior indicates the presence of a tensile strain in the $FeO_2$ region induced by the FeO border. The effect is clearly the most pronounced at the third stage of desorption, at which the departure of oxygen atoms additionally enables a thorough relaxation of the entire FeO lattice and is accompanied by a change of its registry with respect to the Pt(111) surface (Fe cations are on top of surface Pt in the center of the FeO island, whereas both Fe and O ions occupy surface hollow sites at the island boundary). In direct analogy with the embedded case, the presence of such FeO-induced tensile strain reduces the strength of oxygen binding in the $FeO_2$ region, is responsible for the systematically lower $\Delta\varepsilon$ values in the isolated case, and explains the significant reduction of $\Delta\varepsilon$ for the inner oxygen atoms.